

VOLCANOLOGY

The magmatic web beneath Hawai'i

John D. Wilding^{*†}, Weiqiang Zhu[†], Zachary E. Ross, Jennifer M. Jackson

The deep magmatic architecture of the Hawaiian volcanic system is central to understanding the transport of magma from the upper mantle to the individual volcanoes. We leverage advances in earthquake monitoring with deep learning algorithms to image the structures underlying a major mantle earthquake swarm of nearly 200,000 events that rapidly accelerated after the 2018 Kīlauea caldera collapse. At depths of 36 to 43 kilometers, we resolve a 15-kilometers-long collection of near-horizontal sheeted structures that we identify as a sill complex. These sills connect to the lower depths of Kīlauea's plumbing by a 25-kilometers-long belt of seismicity. Additionally, a column of seismicity links the sill complex to a shallow décollement near Mauna Loa. These findings implicate the mantle sill complex as a nexus for magma transport beneath Hawai'i and furthermore indicate widespread magmatic connectivity in the volcanic system.

The structures responsible for transporting magma from the upper mantle to crustal storage chambers have great influence on the dynamical behavior of a volcanic system. These transport structures also encode details about the processes that created them and therefore document the system's history and evolution. The Hawaiian volcanic system has served as a global case study in how many volcanoes grow, erupt, and collapse (1, 2) because of the frequent eruptive activity, the abundance of seismicity, the wealth of instrumentation, and the presence of many volcanoes spanning various stages of life. These factors have led to Hawai'i's Kīlauea Volcano being among the best understood volcanoes in the world, with detailed knowledge of the locations and extent of the magma chambers that supply it (3, 4); detailed knowledge of the geometry of its rift zones (5); and a physical understanding of the eruptive patterns, accompanying seismicity, and geodetic deformation signals (6–8). Despite these major successes, the structures and processes by which magma is transported to these shallow crustal depths remain rather elusive.

Kīlauea's magma supply system is generally believed to follow a near-vertical pathway at shallow depths (9). Although there is geochemical evidence for subcrustal magma storage (10), the magmatic architecture beyond this depth is far less clear, particularly because the current position of the Hawaiian hot spot is believed to be offset from Kīlauea by tens of kilometers (10). A leading idea to explain lateral deep magma transport from the hot spot to Kīlauea is through a set of structures making up a mantle fault zone (11). These structures were first proposed after observations of a persistent, near-horizontal belt of mantle seismicity at ~30- to 35-km depth to the southwest of Kīlauea. This idea was built upon further

by other studies (9, 10, 12, 13) that have argued for the existence of these structures in the upper mantle.

In 2018, Kīlauea experienced its largest caldera collapse and major summit eruption in more than two centuries (2, 14). In August of 2019, ~1 year after the conclusion of this collapse sequence, a marked increase in earthquake swarms at 30- to 40-km depth occurred ~30 km southwest of Kīlauea, near the town of Pāhala (Fig. 1) (15). The depth to the Moho has been estimated at 13 and 18 km underneath Kīlauea and Mauna Loa, respectively, which indicates that the swarms occurred well into the upper mantle (16). The swarms were scattered across a region ~15 km in diameter and close to the area thought to be the current position of the Hawaiian hot spot (9).

To better understand the origin of these Pāhala swarms and how they might relate to the deeper magmatic architecture, we used an earthquake monitoring workflow with deep learning algorithms to reprocess the continuous seismic waveforms across the island and build an extremely detailed seismicity catalog. Imaging the magma plumbing systems from mantle to crust remains challenging for most geophysical methods, such as seismic tomography, geodetic inversion, and gravity and electromagnetic surveys, because these methods typically are unable to resolve the distribution and transportation pathways of magma (17). High-resolution earthquake catalogs built with deep learning provide an unprecedented opportunity to study the detailed spatial and temporal evolution of volcanic earthquake swarms and to characterize the driving mechanisms of magma plumbing systems. The improved picture of magma migration from mantle to crust could thus provide important information for estimating magma intrusion and forecasting volcanic eruption.

Pāhala sill complex

The Pāhala mantle swarm region experienced a notable ~192,000 events over the 3.5-year period. These events span the depth range of

36 to 51 km and can be organized into two main bodies of seismicity that are vertically offset from each other by ~2 km. The upper body (36- to 43-km depth) is primarily composed of volcano-tectonic (VT) earthquakes, whereas the lower body (45- to 51-km depth) is formed of almost exclusively long-period (LP) volcanic earthquakes. The lower body is within the tremor source region identified by Wech and Thelen (12), who interpreted it as a magma-rich volume. The bulk of the seismicity is in the upper body and consists of discrete layered, near-horizontal sheets with typical separation of ~500 m (Fig. 2). Individually, these sheeted structures are as large as 6 km by 5 km with a thickness of up to 300 m. The collection of sheets forms a major regional seismicity feature that extends 17 km laterally across the region and dips ~25° to the west. Although the sheets are predominantly made up of VT earthquakes, they are interspersed with LP volcanic earthquakes. From the totality of these observations, we conclude that the sheeted seismicity structures form a massive complex of mantle sills. Hereafter, we refer to this set of structures as the Pāhala sill complex (PSC), and we subsequently show that it likely serves as a nexus for magmatic activity in the volcanic system.

The seismicity within the PSC exhibits prominent spatiotemporal patterns at multiple scales. The entire volume of seismicity undergoes system-wide surges in the rate of earthquakes along with large-scale migration of seismicity. The largest sills within the PSC, however, individually demonstrate strong variations in event rates and complex patterns of migrating seismicity and quiescence. The disjoint nature of the sills makes them easily extracted with a clustering algorithm. We show the spatial and temporal evolution of the events within four different sills in Fig. 3, with the colors corresponding to the sills in Fig. 2. Spatially migrating swarms initiate within the sills at a single point and expand up, down, or bilaterally along the feature. After their most active phase, many swarms display a back-front of seismic quiescence. Assuming a homogeneous diffusion process from a point source, we can estimate the diffusivity of migrating seismicity (dashed lines in Fig. 3). The estimated point sources, or injection points, are plotted as stars in Fig. 2. We observe a common diffusivity value of ~0.05 m²/s in Fig. 3, A to C, whereas some clusters can migrate at a much faster speed with a diffusivity of 0.54 m²/s (Fig. 3D). In many of the sills, multiple migrating swarms initiate at different times; these later swarms often take place more than a year after the initial swarm began. These repeat episodes in many cases expand the size of the sills beyond the previous dimensions.

Several observations suggest that seismicity within the PSC itself is related to the migration

Seismological Laboratory, California Institute of Technology, Pasadena, CA, USA.

*Corresponding author. Email: jwilding@caltech.edu

†These authors contributed equally to this work.

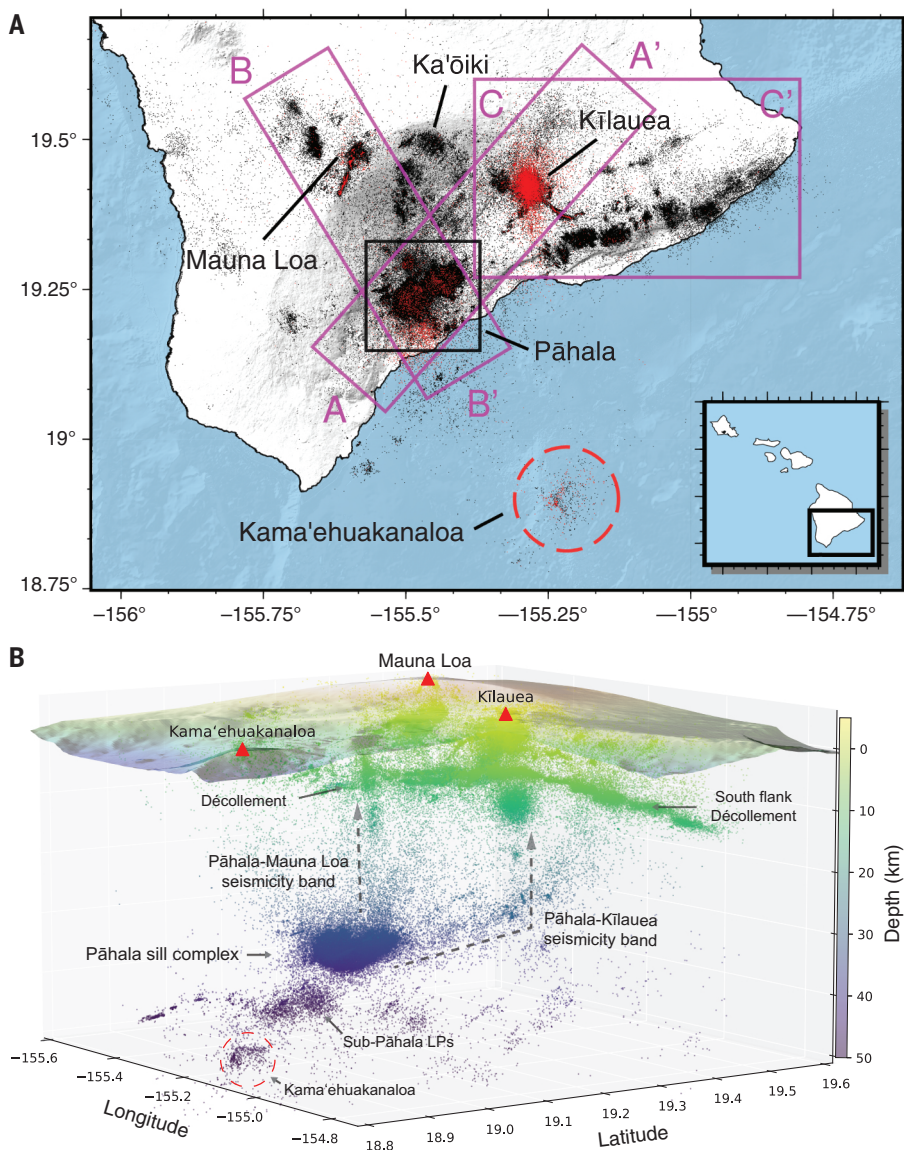


Fig. 1. Overview of seismicity of Hawai'i. (A) Map view of the Island of Hawai'i. Regular earthquakes are colored black, and LP earthquakes are colored red. Cross sections of labeled boxes are plotted in Fig. 5. (B) Three-dimensional view of seismicity colored by depth. Volcanoes are indicated with red triangles.

of magma. Spatiotemporal diffusion of seismicity with accompanying backfronts has previously been linked to transient fluid injection (18). Although static stress transfer (15) could be responsible for generating some of the earthquakes outside of the sills, the multiple discrete fronts of seismicity suggest that seismogenic processes within the structures are more localized. We propose that the observed swarms are generated by the injection of magma into the sills.

The diffuse body of LP earthquake swarms situated beneath the sills at 45- to 51-km depth is the most likely source region for these injected fluids. This LP volume broadly overlaps with a previously identified source region of

impulsive tremor signals and LP seismicity (9, 12, 19). Source mechanisms for LP earthquakes in this volume have been posited as either magma flux through cracks (19) or a volumetrically dispersed stress response to magma influx (12). Degassing of volatile-saturated magmas during decompression has also been proposed as a source mechanism for deep LP earthquakes (20). Any of these source mechanism models allows us to interpret the swarm-like behavior between January 2019 and December 2020 as magmatic unrest preceding apparent fluid injection into the sill complex above. Although LP seismicity is broadly distributed within the sills, its rate of occurrence is highly nonstationary—surges of

LP earthquakes within the sills are only observed after January 2021 (Fig. 4E). This temporal shift in source properties suggests a change in the physical properties of the source region, consistent with growing fluid enrichment in the sills over the time span of our catalog.

The distinctive, sustained intensity of seismic activity within the PSC suggests that material conditions in the source volume are particularly favorable to seismogenesis. Sills in the complex are likely to be composed of mafic magmas with olivine precipitates hosted in a lherzolite matrix (21). The plagioclase-spinel transition in this assemblage has previously been invoked to explain localized seismicity along the mantle fault zone (9). Phase equilibria studies place the maximum depth of this boundary at 30 to 35 km, proximal to the top of the sill complex at 36-km depth (21–23). Over their full depth extent (36 to 43 km), the sills may traverse this boundary, with their uppermost components located in the plagioclase stability region, or they may otherwise be emplaced within a broad plagioclase-spinel coexistence region (21). The location of the sills in this mineralogically complex region suggests that the pronounced seismic activity could be attributed to processes occurring within polyphase magma conduits. Polymimetic assemblages can exhibit transient weakening arising from coupled deformation and metamorphic reactions; this transformation weakening has been observed to promote diffusion creep-based deformation (24) and could facilitate crack growth or fault activation. Although the time scale of this weakening would be limited by the duration of the reaction and the counteracting effect of grain growth, sustained deformation in the PSC may be promoted by recurrent upward injections of magma into the sills. These injections would continuously modulate grain sizes in the PSC, prolonging conditions for seismic deformation in the host rock. This process could exploit lateral variations in strength (25) to produce the laterally compact seismogenic features that we observe.

The speed and intensity with which seismicity migrates throughout the complex suggests the existence of high-permeability paths that can support rapid magma transport. Laboratory experiments on partially molten rocks have demonstrated that melt can segregate into narrow, melt-enriched channels under deformation (26). The substantial melt content of these channels could provide the requisite permeability for the rapid magma transport that we observe; because of their weakness relative to the surrounding mantle, the channels may also serve to localize deformation (27). Our observations suggest that transport channels in the sill complex have attained an advanced stage of development under the

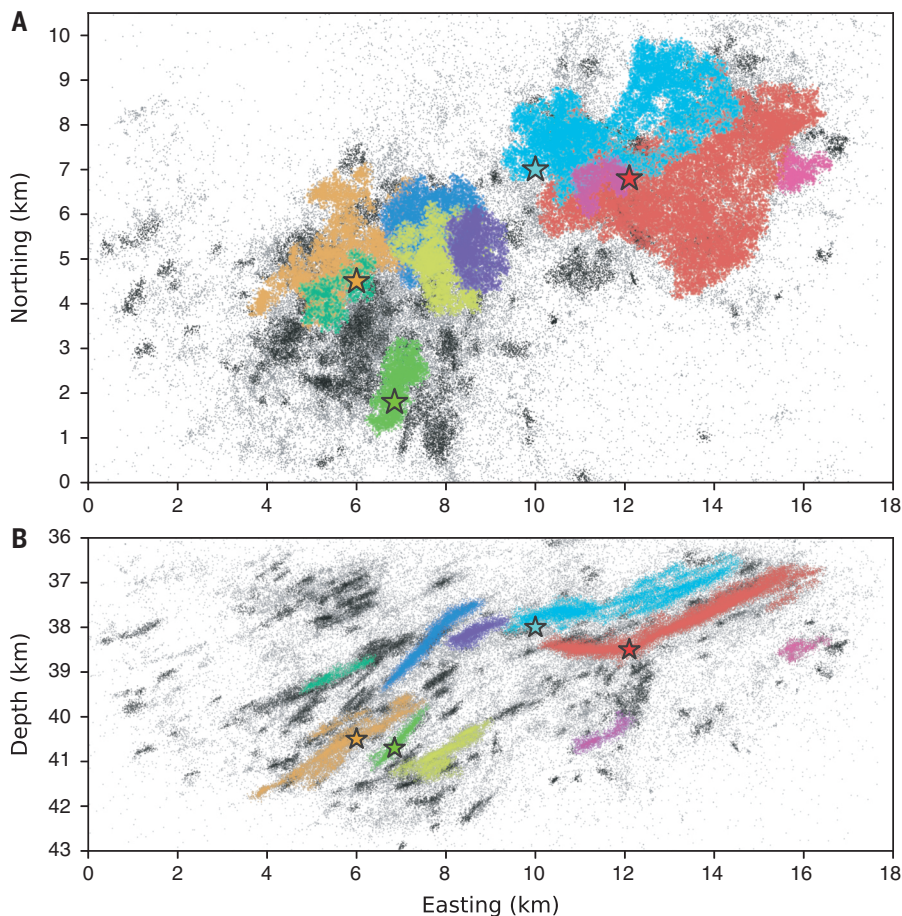


Fig. 2. The geometry of the PSC. (A and B) The map view (A) and cross-sectional view (B) correspond to the black boxed region in Fig. 1. The largest 10 clusters are colored for clarity. The spatiotemporal evolution of four clusters is shown in Fig. 3; the four colored stars are the approximate injection points of each cluster.

effects of long-term shear, possibly from island loading or the motion of the Pacific plate over the hot spot.

The web of seismicity beneath Hawai‘i

At a regional scale, our high-resolution catalog of earthquakes elucidates an interconnected system of seismicity beneath the island of Hawai‘i. Notably, we identify structures emerging from the PSC that connect to the edifices of both Kīlauea and Mauna Loa, which indicates a link between the PSC and both volcanoes.

The sills in the PSC are coplanar with a subhorizontal band of seismicity that extends laterally from the PSC to beneath Kīlauea. These observations are consistent with the hypothesis of a mantle fault zone existing in this region, which has been suggested to serve as a pathway for lateral transport of magma between Kīlauea and the plume (9, 11). Most of the seismicity in this band is characterized by VT earthquakes, but a small cluster of LP earthquakes is present on the seismicity band directly beneath Kīlauea, at 30-km depth. Above these LP earthquakes, there is a near-

vertical trend of seismicity that extends upward to ~20-km depth. This trend terminates just below a large cluster of LP seismicity at 10- to 15-km depth (Fig. 5A). To the northeast of Kīlauea, another branch of the structure abruptly deflects upward and rises nearly vertically to meet the surface. We refer to this overall band of seismicity as the Pāhala-Kīlauea seismicity band (Fig. 5A).

A second distinct seismicity structure connects the PSC to the Mauna Loa edifice, which we refer to as the Pāhala-Mauna Loa seismicity band. This 25-km-long column of seismicity rises from the northern edge of the PSC to the décollement beneath the Ka‘ōiki seismic zone at a depth of 10 km, 20 km south of the Mauna Loa summit (Fig. 5B). The location of the Pāhala-Mauna Loa seismicity band is consistent with a previously proposed magma transport path between the PSC region and the Mauna Loa edifice (9). Although this path was inferred from the geometry of seismicity at 30-km depth, our catalog captures the first identified continuous structure that connects the two regions.

We also observe a collection of deep LP earthquakes almost directly beneath Kama‘ehuakanaloa Volcano (formerly Lō‘ihī) at 50-km depth (Fig. 1). Although deep seismicity has been observed beneath Kama‘ehuakanaloa, it has previously been interpreted as belonging to a diffuse zone of seismicity between 20- and 60-km depth (28). Our catalog allows us to identify these events as LPs that are distinctly concentrated deep beneath the summit of Kama‘ehuakanaloa. On the basis of their colocation with the Kama‘ehuakanaloa summit, we suggest that these deep LPs represent a deep part of the volcano’s magma system, as has been similarly inferred from LPs detected beneath Kīlauea and Mauna Loa (9, 29). Our catalog also reproduces a concentrated volume of deep LP seismicity beneath Mauna Kea that has previously been attributed to second boiling of a stalled magma body (fig. S4) (30).

Systemic interconnectivity

The spatiotemporal patterns of seismicity within the aforementioned structures are closely linked. The rates of earthquake activity and their source properties are seen to undergo rapid changes in response to distal eruptive activity or changes elsewhere in the system (Fig. 4).

Several episodic LP earthquake swarms took place in the seismicity body beneath the PSC between January and August 2019 (Fig. 4F). In July 2019, a week-long swarm of LP earthquakes occurred on the Pāhala-Kīlauea seismicity band, directly beneath Pāhala at 30-km depth (Fig. 4B). This episode coincided with an order-of-magnitude increase of VT seismicity rates within the PSC, 25 km away (Fig. 4D). During this phase of activity, multiple discrete swarms of VT seismicity migrated upward and to the east along the sills; this activity represents the first activation of these structures in our catalog. Simultaneously, the rate of earthquakes in Kīlauea’s east rift zone steadily began to increase, from a mean of 15 events per week to values as high as 436 events per week during December 2020 (Fig. 4A).

After this activity, Kīlauea experienced two eruptions in late December 2020 and September 2021 (31, 32). Several features throughout the volcanic system responded immediately to these eruptions. At the onset of both eruptions, the rate of activity at Kīlauea’s summit shut down and remained quiescent for months. After the 2020 eruption, the PSC immediately experienced a substantial increase in the rate of VT and LP earthquakes, which formed migrating swarms suggestive of fluid injection into the sills. After the 2021 eruption, the PSC experienced another episode of migratory swarms along with acceleration in the rate of LP earthquakes. These LP earthquakes occur

along the same sill structures generated during the previous stages of VT seismicity.

Both the Kīlauea and Mauna Loa seismicity bands experienced earthquake rate increases after the 2020 and 2021 Kīlauea eruptions. The rate increases after the 2020 eruption were gradual and occurred over months. After the 2021 eruption, the rate increases in both structures instead occurred over weeks (Fig. 4).

Discussion

Although our findings have important implications for large-scale magma transport in the system, particularly with regards to the forecasting of eruptive activity, magma transport in the Hawaiian mantle is likely not the sole process behind seismogenesis at these depths. Flexural or loading stresses are a viable mechanism for generating VT mantle seismicity (3, 13). In contrast to the broadly distributed seismicity expected from these stresses (3, 13), the Pāhala-Kīlauea and Pāhala-Mauna Loa seismicity bands revealed by our catalog are spatially concentrated features along previously theorized magma transport routes. In particular, the columnar structures beneath both volcanoes are suggestive of an additional, localized source of stress at depth.

Furthermore, previously observed or theorized magmatic structures are connected along the seismicity bands. Both bands originate from the magmatic PSC. The Pāhala-Kīlauea band rises to meet a concentrated volume of LP seismicity beneath Kīlauea's summit at 10- to 15-km depth (Fig. 5A), a persistent feature that has been interpreted as part of its magma system (33). LP earthquakes at 30-km depth additionally suggest the presence of magma or magmatic fluids deeper within the vertical column beneath the volcano. The Pāhala-Mauna Loa band terminates at the décollement within the Ka'ōiki seismic zone; a concentration of LP earthquakes is present within this intersecting region at 10-km depth (Fig. 5B). Although seismicity above this intersection is diffuse, the location of these LPs is connected to the summit by a positive *P*-wave velocity anomaly that has been interpreted as ultramafic cumulates associated with crustal magma storage (9, 34).

From these observations, we interpret the seismicity bands as magmatic structures connecting Kīlauea and Mauna Loa to a common source in the mantle (Fig. 6). Earthquakes occurring throughout the bands could be stimulated by the localized addition of magmatic stressing to background flexural and tectonic stress (11). The rapid response of the PSC to the July 2019 LP earthquake swarm and Kīlauea's 2020 and 2021 eruptions would suggest that system-wide pressure gradients can propagate quickly through the system, as observed in other regions, such as beneath Kamchatka volcanoes (35, 36).

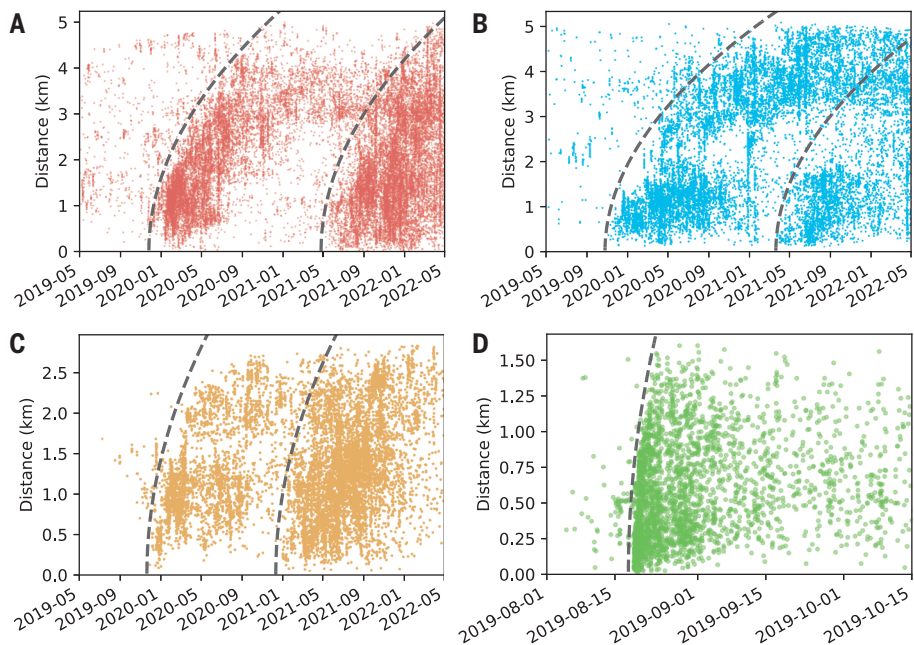


Fig. 3. Spatiotemporal evolution of the Pāhala sill seismicity. (A to D) The distance is calculated from the injection points indicated by stars in Fig. 2. The dashed lines are the diffusion fronts, assuming a homogeneous media with a diffusivity value of $0.05 \text{ m}^2/\text{s}$ [(A) to (C)] and $0.54 \text{ m}^2/\text{s}$ (D).

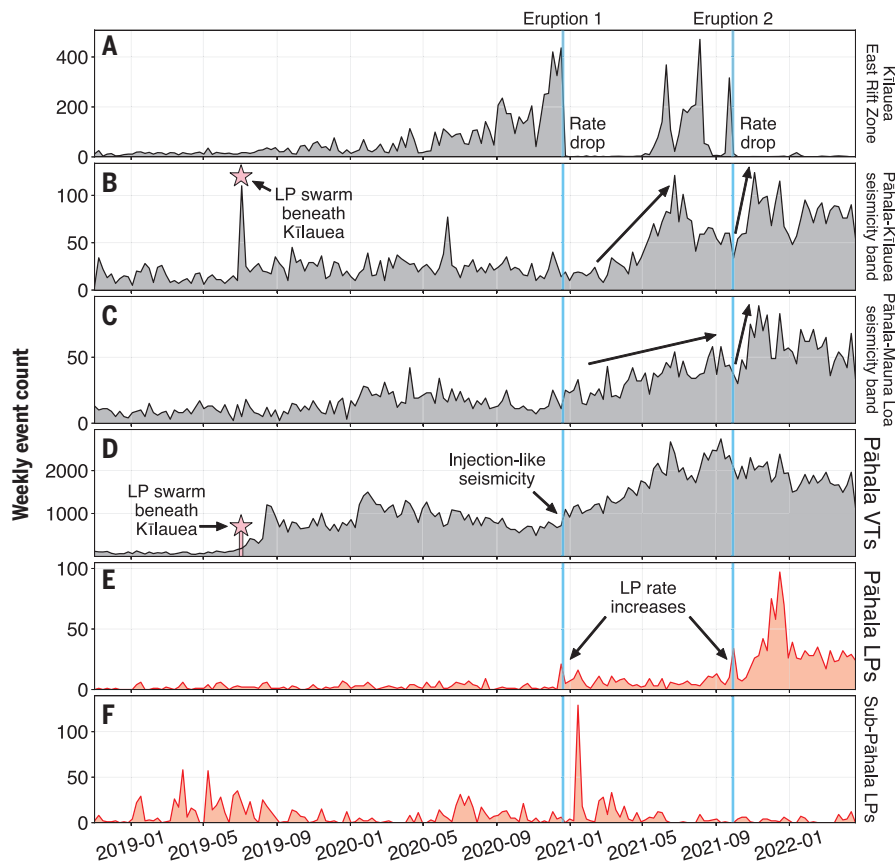
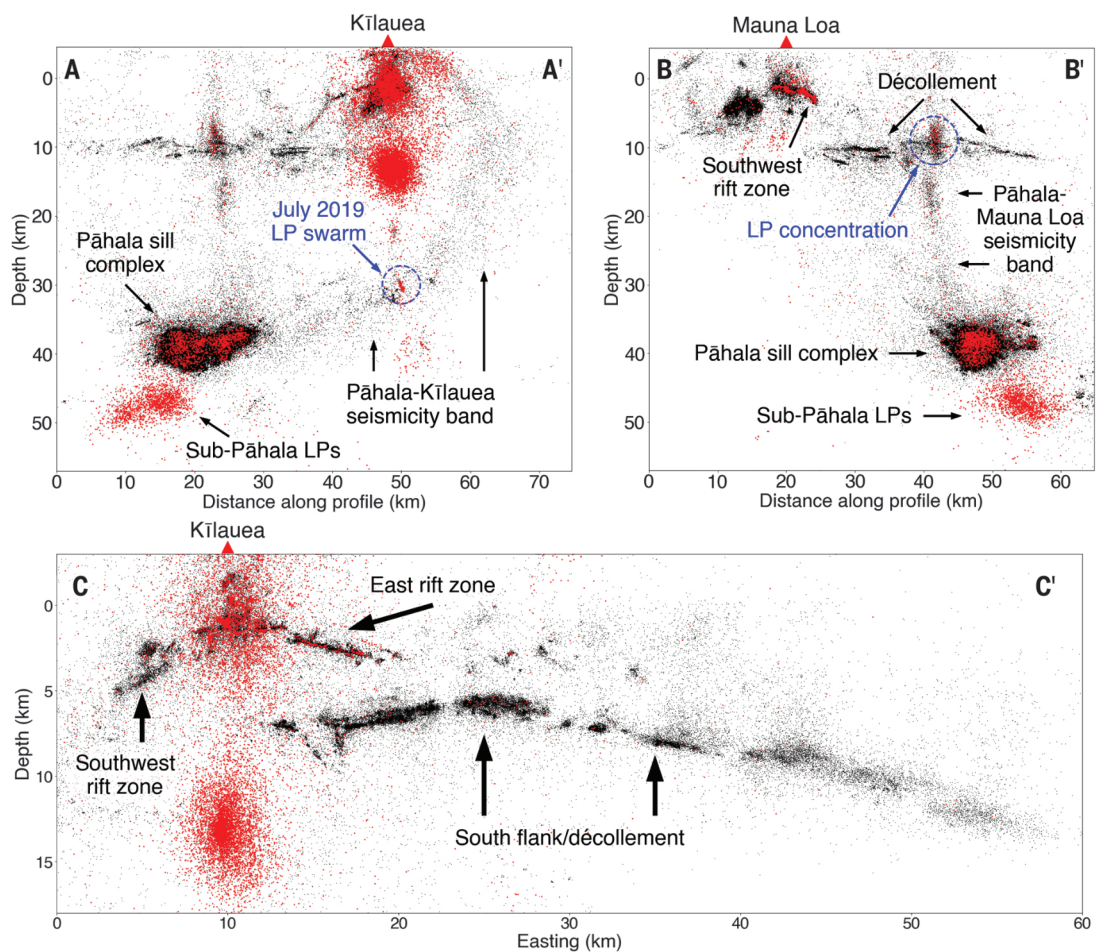


Fig. 4. Temporal variation of event counts for various regions making up the magmatic system. (A to F) The 2020 and 2021 eruptions at Kīlauea are demarcated by cyan lines. Pāhala VTS and Pāhala LPs refer to VT and LP earthquakes within the PSC, respectively. Sub-Pāhala LPs refers to the distributed volume of LP earthquakes beneath the sill complex.

Fig. 5. Depth sections of seismicity.

seismicity. The individual cross sections show seismicity within the boxes plotted in Fig. 1. VT seismicity is shown in black; LP seismicity is shown in red with larger marker size to emphasize its distribution. **(A)** Seismicity along the Pāhala-Kīlauea profile, A to A'. **(B)** Seismicity along the Pāhala-Mauna Loa profile, B to B'. **(C)** Shallow seismicity within the Kīlauea edifice, C to C'.



After PSC intrusions, increasing earthquake rates within the Pāhala-Kīlauea and Pāhala-Mauna Loa seismicity bands could plausibly be attributed to increased flux of magma or magmatic fluids between the PSC and the surface. Alternatively, accelerating earthquake rates within the seismicity bands could reflect intensifying VT activity within the crustal edifices of Kīlauea and Mauna Loa accompanied by broad-scale deformation that may stress the mantle below (3).

The PSC may serve as a common magma source at 40-km depth for Kīlauea and Mauna Loa. This degree of volcanic interconnectivity is noteworthy in light of geochemical and past seismological results that imply Hawaiian volcanoes have distinct plumbing systems sourced from distinct regions of the underlying plume (9, 29, 37–39). The seismic structures we observe suggest that previously posited magma transport routes may be nonunique; the connection between the deep tremor region (12) and the volcanoes may represent one part of a distributed network of structures.

Temporal clustering of eruptive behavior between neighboring volcanoes is well documented (40). In the absence of evidence of shallow magmatic connections, such cluster-

ing has been attributed to stress transfer (40, 41) or has been proposed to be an artifact caused by spatial clustering of volcanoes in plate boundary regions (42). Our results suggest that many neighboring volcanoes might have more extensively connected magma systems than has previously been appreciated.

The apparent absence of large, seismogenic magma structures beneath Kama'ehuakanaloa could reflect the volcano's distance from the hot spot. The local geotherm might not intersect the solidus above 50-km depth so that persistent magma storage at shallower depths is not thermodynamically viable. A purely vertical magmatic architecture beneath Kama'ehuakanaloa would suggest that formation of lateral transport structures in the uppermost mantle (<50 km) is not favored at earlier stages of a Hawaiian volcano's life cycle. Such connections might only become favorable after the development of laterally extensive magma systems (43) under the effects of long-term shear.

Many prior attempts to image magmatic structures underneath the island of Hawai'i have used seismic tomography methods (44), which have limited sensitivity to fine-scale structure. However, microseismicity enables us to characterize connections between mag-

matic structures with high precision (45). Our seismicity catalog also captures detailed patterns of unrest in the shallow magma systems of Kīlauea and Mauna Loa. A substantial proportion of LP earthquakes are detected within Kīlauea's summit and east rift zone, as well as Mauna Loa's summit and southwest rift zone. LP earthquake locations in these features are spatially concentrated, consistent with previous observations (33, 46). Although rift zone swarms may be triggered tectonically (7) and do not necessarily portend eruptive activity, the patterns of activity that we observe highlight the possibility of enhanced monitoring and eruptive forecasting with microseismicity catalogs as well as the improved characterization of shallow reservoir systems.

Our analysis of the Pāhala swarm is the first *in situ* observation of magma dynamics in the mantle at the resolution of individual structures. These measurements represent a rich opportunity to study diffusion and emplacement models at remote depths in future work. Although the observed swarm in the PSC should be viewed as a major sequence in this volcanic system, it is probably not unique. Comparable mantle swarms occurred during 1953 to 1960 beneath Kīlauea, a period of

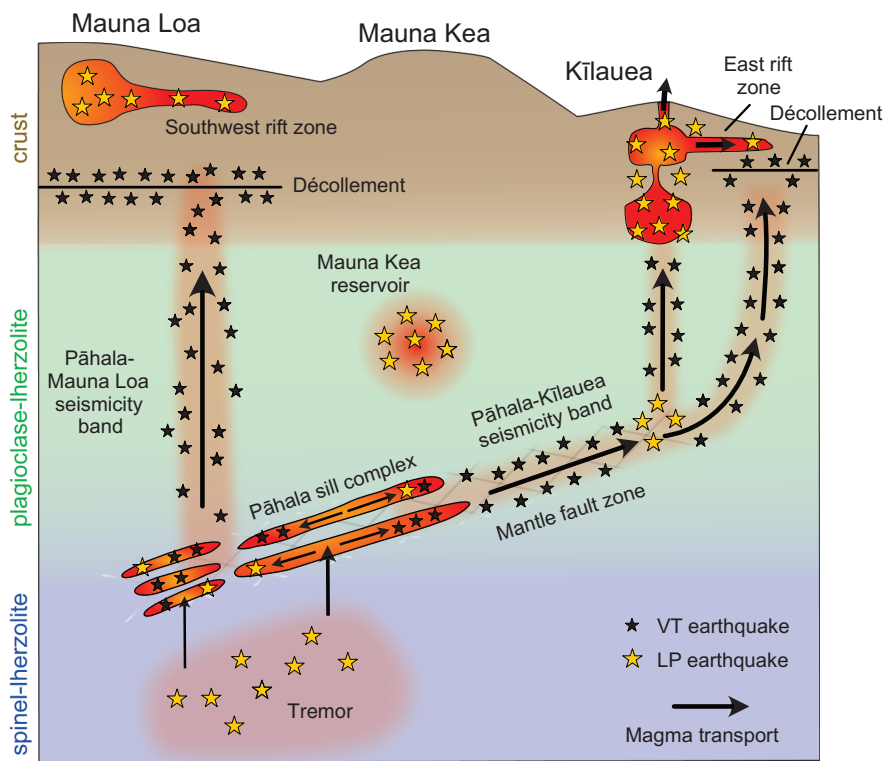


Fig. 6. Cartoon summarizing observations. Eruptions and intrusions at Kilauea cause pressure gradients to rapidly propagate through the Kilauea transport structure to the PSC. Magma is injected into the PSC from the underlying magma-bearing volume; the sills are proximal to the plagioclase-spinel phase boundary, possibly in a polyphase coexistence region. The sills are connected to Kilauea and the décollement or Ka'ōiki region within the Mauna Loa edifice along continuous bands of seismicity.

time that includes the 1959 to 1960 Kilauea Iki eruption. Although hypocenters from this era of Hawai'i monitoring are not well constrained by modern standards, the depth of this swarm sequence has been estimated at 45 to 65 km, well into the mantle (47). Although this earlier swarm might have originated in the structures that we image, the apparent nonuniqueness of deep magma transport paths under Hawai'i raises the possibility of activity within a distinct set of structures. The size and level of activity observed within the PSC suggest that these features may be important contributors to the growth process of Hawaiian volcanoes and therefore may encode valuable historical information about plume-surface interaction.

Similar mantle earthquake swarms have been reported at several other ocean island volcanoes, including Fogo, El Hierro, and La Réunion (48–50). In particular, the Fogo swarm took place at similar depths (38 to 44 km) to the PSC swarm and has been interpreted as sill emplacement. These observations hint that large-scale mantle magma transport structures like the PSC may be present under many other ocean island volcanoes. Future improvements to earthquake monitoring capabilities

could facilitate better identification of connections between deep magma and surface volcanoes, with important implications for real-time monitoring.

REFERENCES AND NOTES

- J. G. Moore, D. A. Clague, *Geol. Soc. Am. Bull.* **104**, 1471–1484 (1992).
- C. A. Neal et al., *Science* **363**, 367–374 (2019).
- F. W. Klein, R. Y. Koyanagi, J. S. Nakata, W. R. Tanigawa, in *Volcanism in Hawaii: Volume 2*, R. W. Decker, T. L. Wright, P. H. Stauffer, Eds. (US Geological Survey, professional paper 1350, 1987), pp. 1019–1185.
- A. F. Flinders et al., *Geophys. Res. Lett.* **40**, 3367–3373 (2013).
- D. Gillard, A. M. Rubin, P. Okubo, *Nature* **384**, 343–346 (1996).
- E. K. Montgomery-Brown, A. Miklius, *Geology* **49**, 397–401 (2020).
- C. Wauthier, D. C. Roman, M. P. Poland, *Geology* **47**, 820–824 (2019).
- B. Chouet, P. Dawson, *J. Geophys. Res.* **116**, B12317 (2011).
- T. L. Wright, F. W. Klein, *Lithos* **87**, 50–79 (2006).
- K. Putirka, *Geology* **25**, 69 (1997).
- C. J. Wolfe, P. G. Okubo, P. M. Shearer, *Science* **300**, 478–480 (2003).
- A. G. Wech, W. A. Thelen, *Geophys. Res. Lett.* **42**, 7090–7097 (2015).
- M. E. Pritchard, A. M. Rubin, C. J. Wolfe, *Geophys. J. Int.* **168**, 419–430 (2007).
- K. R. Anderson et al., *Science* **366**, eaaz1822 (2019).
- M. K. Burgess, D. C. Roman, *Geophys. Res. Lett.* **48**, e2020GL091096 (2021).
- D. P. Hill, J. J. Zucca, in *Volcanism in Hawaii: Volume 2*, R. W. Decker, T. L. Wright, P. H. Stauffer, Eds. (US Geological Survey, professional paper 1350, 1987), pp. 903–917.
- C. Magee et al., *J. Petrol.* **59**, 1217–1251 (2018).
- Z. E. Ross, E. S. Cochran, *Geophys. Res. Lett.* **48**, e2021GL092465 (2021).
- K. Aki, R. Koyanagi, *J. Geophys. Res.* **86**, 7095–7109 (1981).
- O. Melnik, V. Lyakhovsky, N. M. Shapiro, N. Galina, O. Bergal-Kuvikas, *Nat. Commun.* **11**, 3918 (2020).
- G. Sen, *Earth Planet. Sci. Lett.* **62**, 215–228 (1983).
- G. Borghini, P. Fumagalli, E. Rampone, *J. Petrol.* **51**, 229–254 (2010).
- P. Wyllie, *Geol. Rundsch.* **70**, 128–153 (1981).
- H. Stünitz et al., *J. Struct. Geol.* **139**, 104129 (2020).
- A. Bellas, S. J. Zhong, *Geochem. Geophys. Geosyst.* **22**, e2020GC009547 (2021).
- B. K. Holtzman, N. J. Groebner, M. E. Zimmerman, S. B. Ginsberg, D. L. Kohlstedt, *Geochem. Geophys. Geosyst.* **4**, 8607 (2003).
- M. E. Zimmerman, D. L. Kohlstedt, *J. Petrol.* **45**, 275–298 (2004).
- F. W. Klein, *J. Geophys. Res.* **87**, 7719–7726 (1982).
- P. G. Okubo, C. J. Wolfe, *J. Volcanol. Geotherm. Res.* **178**, 787–794 (2008).
- A. G. Wech, W. A. Thelen, A. M. Thomas, *Science* **368**, 775–779 (2020).
- P. Segall, K. Anderson, T. A. Wang, *Geophys. Res. Lett.* **49**, e2022GL099270 (2022).
- Global Volcanism Program, “Report on Kilauea (United States),” K. L. Bennis, E. Venzke, Eds., *Bulletin of the Global Volcanism Network*, 47:1 (Smithsonian Institution, 2022).
- R. S. Mattoza, P. M. Shearer, P. G. Okubo, *Geophys. Res. Lett.* **41**, 3413–3421 (2014).
- P. G. Okubo, H. M. Benz, B. A. Chouet, *Geology* **25**, 867 (1997).
- C. Journeau et al., *Sci. Adv.* **8**, eabj1571 (2022).
- N. M. Shapiro et al., *Nat. Geosci.* **10**, 442–445 (2017).
- J. E. Dixon, D. A. Clague, E. M. Stolper, *J. Geol.* **99**, 371–394 (1991).
- J. M. Rhodes, K. P. Wenz, C. A. Neal, J. W. Sparks, J. P. Lockwood, *Nature* **337**, 257–260 (1989).
- F. A. Frey, J. M. Rhodes, K. G. Cox, D. P. McKenzie, R. S. White, *Phil. Trans. R. Soc. A* **342**, 121–136 (1993).
- A. T. Linde, I. S. Sacks, *Nature* **395**, 888–890 (1998).
- H. M. Gonnermann et al., *Nat. Geosci.* **5**, 826–829 (2012).
- D. M. Palladino, G. Sottilli, *Geophys. Res. Lett.* **39**, L12308 (2012).
- R. S. J. Sparks et al., *Phil. Trans. R. Soc. A* **377**, 20180019 (2019).
- G. Lin, P. M. Shearer, F. Amelung, P. G. Okubo, *J. Geophys. Res. Solid Earth* **120**, 2510–2524 (2015).
- A. J. Hotovec-Ellis et al., *Sci. Adv.* **4**, eaat5258 (2018).
- J. Battaglia, J.-L. Got, P. Okubo, *J. Geophys. Res.* **108**, 2553 (2003).
- J. P. Eaton, D. H. Richter, H. L. Krivoy, in *Volcanism in Hawaii: Volume 2*, R. W. Decker, T. L. Wright, P. H. Stauffer, Eds. (US Geological Survey, professional paper 1350, 1987), pp. 1307–1335.
- C. Leva, G. Rümpker, F. Link, I. Wölbern, *J. Volcanol. Geotherm. Res.* **386**, 106672 (2019).
- A. Klügel, M.-A. Longpré, L. García-Cañada, J. Stix, *Earth Planet. Sci. Lett.* **431**, 140–149 (2015).
- Z. Duputel et al., *C. R. Geosci.* **353**, 237–255 (2021).

ACKNOWLEDGMENTS

The authors acknowledge comments by A. Flinders and an anonymous reviewer that substantially improved the manuscript. The facilities of IRIS Data Services, and specifically the IRIS Data Management Center (DMC), were used for access to waveforms, related metadata, and/or derived products used in this study. IRIS Data Services are funded through the Seismological Facilities for the Advancement of Geoscience (SAGE) Award of the National Science Foundation under cooperative support agreement EAR-1851048. The computations presented in this work were conducted

in the Resnick High Performance Computing Center, a facility supported by the Resnick Sustainability Institute at the California Institute of Technology. **Funding:** Z.E.R. and J.D.W. received support from NSF award EAR-2034167. J.M.J. acknowledges the JPL Strategic Research & Technology Development Program, “Venus Science Into The Next Decade.” **Author contributions:** W.Z. performed phase picking. Z.E.R. and J.D.W. performed quality control on the phase picks and constructed the catalog. Z.E.R. and W.Z. performed earthquake relocation. J.D.W. performed the frequency index calculations. J.D.W., W.Z., Z.E.R., and J.M.J.

contributed to data analysis and writing. All authors contributed to the revised version of the manuscript. **Competing interests:** All authors declare no competing interests. **Data and materials availability:** Seismic data are publicly available from the IRIS DMC. The seismicity catalog developed in this study will be made publicly available. **License information:** Copyright © 2023 the authors, some rights reserved; exclusive licensee American Association for the Advancement of Science. No claim to original US government works. <https://www.science.org/about/science-licenses-journal-article-reuse>

SUPPLEMENTARY MATERIALS

science.org/doi/10.1126/science.adc5755

Materials and Methods

Figs. S1 to S12

References (51–89)

Movie S1

Data S1

Submitted 24 August 2022; accepted 8 December 2022
10.1126/science.adc5755

NEUROSCIENCE

Suppressing feedback signals to visual cortex abolishes attentional modulation

Samantha R. Debes¹ and Valentin Dragoi^{1,2*}

Attention improves perception by enhancing the neural encoding of sensory information. A long-standing hypothesis is that cortical feedback projections carry top-down signals to influence sensory coding. However, this hypothesis has never been tested to establish causal links. We used viral tools to label feedback connections from cortical area V4 targeting early visual cortex (area V1). While monkeys performed a visual–spatial attention task, inactivating feedback axonal terminals in V1 without altering local intracortical and feedforward inputs reduced the response gain of single cells and impaired the accuracy of neural populations for encoding external stimuli. These effects are primarily manifested in the superficial layers of V1 and propagate to downstream area V4. Attention enhances sensory coding across visual cortex by specifically altering the strength of corticocortical feedback in a layer-dependent manner.

Selective attention is a critical brain mechanism that enhances the processing of relevant sensory information. Attentional modulation of sensory encoding, intensively studied over the past several decades, has long been hypothesized to originate from downstream areas carrying top-down feedback signals to early cortex such as to increase response gain, sensitivity, and accuracy of network computations (1–4). Understanding the neural mechanisms of attentional modulation depends on our ability to activate or silence presynaptic downstream areas and subsequently assess their impact on the target network. However, separating the impact of feedback inputs from local intracortical and bottom-up inputs, which is necessary for examining the mechanism of top-down attentional modulation, has been challenging when using traditional neuromodulation methods (1–11). Here, we combined *in vivo* electrophysiology in behaving monkeys with an optogenetic protocol to perturb construct-expressing neuronal processes and modulate feedback signals without altering the strength of feedforward and intracortical inputs that are not directly caused by feedback.

To examine the function of corticocortical feedback for attentional modulation of sensory coding, we have chosen a major pathway

involving primary and midlevel visual cortical areas V1 and V4 in behaving monkeys. Neurons in V4 carry top-down signals related to behavioral context and attention to V1 via direct, monosynaptic feedback projections (12–16). Although V1 also receives feedback inputs from area V2, neurons in V4 are more strongly modulated by attention and are hierarchically closer to decision-making areas; hence, they are ideally suited to examine the impact of cortical feedback on the transmission of attentional signals to early cortex (17, 18).

Results

We developed a sensitive assay based on viral-mediated labeling of feedback connections arising from midlevel cortical area V4 that target area V1. The construct leveraged a halorhodopsin-derived chloride pump, Jaws, in adeno-associated virus serotype 8 (AAV8) under the control of the promoter human synapsin (19, 20). AAV8-hSyn-Jaws-GFP-ER2 was expressed within an approximately 12.6-mm³ cortical volume in area V4 (Fig. 1A) (see materials and methods). This allowed us to simultaneously place a linear electrode array and fiber optic in V1 to record neural activity at multiple sites (fig. S1) and selectively suppress axonal feedback terminals of V4 neurons targeting V1 while macaques performed a spatial attention task. Because the viral construct was injected in V4, we reasoned that shining red light in the superficial layers of V1 would specifically inactivate feedback inputs while leaving un-

perturbed local intracortical and feedforward inputs to V1 neurons (Fig. 1A). This allowed us to examine whether the attentional modulation of neural populations in V1 is impaired when suppressing cortical feedback from V4 and whether the hypothesized reduction in attentional modulation in V1 is further transmitted to postsynaptic V4 targets.

Optogenetic suppression of V4 feedback axons in V1

Two monkeys performed a spatial-attention contrast detection task (Fig. 1B and fig. S2) whereby various contrast stimuli were displayed at two symmetric spatial locations on a computer screen. One location covered the receptive fields of the neurons being recorded and the other location was outside the receptive fields, diametrically opposed at the same eccentricity. Only one spatial location was behaviorally relevant on a given trial: Monkeys were cued by the color of the fixation point to attend to the stimuli covering the neurons’ receptive fields or to those presented on the contralateral side (see materials and methods) (Fig. 1B). On 50% of trials in each condition, optical stimulation was applied to selectively suppress V4 feedback axons in the upper layers of V1. To maintain equal behavioral performance in the “laser” and control conditions, we restricted laser power to a low level such that behavioral performance at the attended side was not significantly different between control and laser trials ($P = 0.52$) (Fig. 1B); these effects were consistent across animals (fig. S3), and perceptual performance was unaffected by the stimuli flashed at the unattended location (fig. S4). If light stimulation would change behavioral performance across conditions, the obtained unequal reward across conditions could possibly alter behavioral context and hence introduce additional top-down feedback signals besides those related to attention. The lack of a behavioral effect in the laser condition may be due to the fact that in monkey cortex, only a fraction of neurons at the injection site are typically transfected (21), and this likely resulted in a small number of cells that were perturbed relative to the entire V1 population encoding the stimuli.

We first placed the electrode array and fiber optic at the injection site in V4, which was associated with a direct suppression of local

¹Department of Neurobiology and Anatomy, McGovern Medical School, University of Texas at Houston, Houston, TX 77030, USA. ²Department of Electrical and Computer Engineering, Rice University, Houston, TX 77005, USA.

*Corresponding author: Email: valentin.dragoi@uth.tmc.edu

Copyright 2023 American Association for the Advancement of Science. All rights reserved.